Fermi-surface instabilities and superconducting d-wave pairing

D. J. Scalapino and E. Loh, Jr.*

Department of Physics, University of California, Santa Barbara, California 93106

J. E. Hirsch

Department of Physics, University of California, San Diego, California 92093

(Received 11 August 1986)

Near nesting of the Fermi surface can lead to low-frequency spin-density, charge-density and lattice modes at wave vectors connecting the nested regions. We find that the exchange of these excitations leads to a superconducting coupling constant for d-wave pairing which is enhanced near the Fermi-surface instability.

I. INTRODUCTION

Fermi-surface nesting or near nesting can lead to a variety of instabilities involving Peierls, charge-density-wave (CDW) and spin-density-wave (SDW) instabilities. It has been argued that the high superconducting transition temperatures of the $A15$ compounds arise from an insipient Peierls-driven martensitic instability.[1] Various theoretical models[1-3] of this phenomena based on s-wave pairing arising from the exchange of soft phonons have been discussed. Recently, the superconducting heavy-fermion material UPt_3 has been shown to be near a Fermi-surface instability associated with a spin-density wave.[4] The Bechgaard salt $(TMTSF)_2AsF_6$ was shown to exhibit a pressure-dependent SDW Fermi-surface instability adjacent to its superconducting phase.[5] In these cases, an alternate pairing mechanism involving the exchange of spin-density waves[6-9] may occur. Béal-Monod *et al.*[10] have recently examined this mechanism for a rotationally invariant model. They find that if the system is nearly antiferromagnetic with a large wave vector $|q_0|$ (corresponding to backward scattering), the paramagnon-mediated interaction is repulsive, leading to a suppression of both triplet and singlet pairing. However, we have studied a Hubbard model on a cubic lattice[8] and found that, within a random-phase-approximation (RPA) treatment of the SDW response, the singlet d-wave pairing interaction is, in fact, attractive when the SDW instability is approached while the triplet p-wave interaction is repulsive.[11] Here we describe these calculations and extend them to discuss pairing near CDW and Peierls instabilities in the presence of a strong on-site Coulomb repulsion.

The model we will discuss has a cubic lattice with a near-neighbor hopping parameter t leading to the simple band structure

$$E_p = -2t\,(\cos p_x + \cos p_y + \cos p_z)\ .$$

The pairing interactions are obtained from the basis Coulomb or electron-phonon interactions within an RPA approximation. For example, in the SDW case, an on-site repulsive Coulomb coupling $Un_{i\uparrow}n_{i\downarrow}$ provides the basic interaction, and we have a three-dimensional (3D) Hubbard model. In the CDW case, a near-neighbor Coulomb interaction Vn_in_j is added, giving an extended Hubbard model, and the charge fluctuations are assumed to dominate over the spin fluctuations. For the Peierls case, an electron-phonon coupling is added. Clearly, this is basically a phenomenological approach. In particular, an RPA treatment typically overestimates the response, and in a strongly interacting fermion system the designation of the response as SDW or CDW may itself be misleading. Thus in a periodic Anderson model one may be dealing with hybridization fluctuations between the conduction and the nearly localized f electrons.[12,13] Nevertheless, an RPA approach provides a framework within which one can clearly see the effect of Fermi-surface nesting on the interaction. Since we believe that the degree of nesting is an essential feature, giving the pairing interaction a unique spatial structure and strength, it seems worthwhile to explore the consequences of a simple model viewing the parameters which enter as phenomenological.

Retardation plays a central role in the pairing interaction and, just as in the Eliashberg theory for the electron-phonon interaction,[14,15] one introduces Fermi-surface-averaged spectral weights of the effective interaction $V(p',p,\omega)$,

$$F(\omega) = \left\langle -\frac{1}{\pi}\mathrm{Im}\,V(p',p,\omega)\right\rangle\ . \tag{1}$$

These Fermi-surface averages depend upon the form of the pairing as discussed below. From these spectral weights one can determine the superconducting transition temperature. Here, however, we will focus on one moment of $F(\omega)$,

$$\lambda = 2\int_0^\infty d\omega\,\frac{F(\omega)}{\omega}\ , \tag{2}$$

which characterizes the strength of the pairing interaction in a given channel. Substituting Eq. (1) into Eq. (2) and using the Kramers-Kronig relation, one finds that

$$\lambda = -\langle\mathrm{Re}\,V(p',p,0)\rangle\ . \tag{3}$$

Thus, in the following analysis we will need the zero-frequency limit of the effective interaction.

© 1987 The American Physical Society

To model the SDW pairing mechanism, we consider a 3D Hubbard model with a repulsive on-site Coulomb interaction U. A RPA treatment of the spin susceptibility $X(q)$ leads to the condition

$$1 = U X_0(q) \tag{4}$$

for a SDW instability. Here,

$$X_0(q) = \sum_k \frac{f(\epsilon_{k+q}) - f(\epsilon_k)}{\epsilon_k - \epsilon_{k+q}} , \tag{5}$$

with

$$\epsilon_k = -2t (\cos k_x + \cos k_y + \cos k_z) - \mu$$

for a cubic tight-binding band. As is well known, for a half-filled band ($\mu = 0$) the Fermi surface has perfect nesting for $q^* = (\pm \pi, \pm \pi, \pm \pi)$. At this wave vector $X(q^*)$ grows logarithmically at low temperatures varying as $\ln(t/T)$, so that, for any value of U, Eq. (4) can always be satisfied at some finite T. For $\mu \neq 0$, $X(q)$ has a finite maximum at zero temperature which diverges as $\ln(t/\mu)$ when $\mu \to 0$. In this case, for a fixed value of U in Eq. (4), there will be a critical value of μ such that

$$1 = U X_0(q^*, \mu_c, T = 0) . \tag{6}$$

Here we are interested in studying the pairing interaction which is mediated by the exchange of paramagnon spin-density waves for μ below μ_c. We will also assume that the superconducting transition occurs at sufficiently low temperatures that X_0 is essentially equal to its $T = 0$ value.

The basic RPA pairing interactions are illustrated in Fig. 1. Particle-hole scattering and the screened Coulomb interaction give the even-parity singlet-pairing potential

$$V_s = U + \frac{U^3 X_0^2(p'-p)}{1 - U^2 X_0^2(p'-p)} + \frac{U^2 X_0(p'+p)}{1 - U X_0(p'+p)} . \tag{7}$$

Here the static Coulomb part U has been separated from the paramagnon terms. In this same approximation, the triplet pairing potential is

$$V_t = -\frac{U^2 X_0(p'-p)}{1 - U^2 X_0^2(p'-p)} . \tag{8}$$

Just as one projects out the Y_{lm} parts of the interaction for the continuum case, it is useful to use tight-binding cubic harmonics to decompose V_s and V_t. Here we will use the s-wave-like functions

$$g_0(p) = 1 \tag{9a}$$

FIG. 1. The paramagnon contributions to the even-parity singlet V_s and odd-parity triplet V_t pairing channels.

and

$$g_{s^*}(p) = A + (\cos p_x + \cos p_y + \cos p_z) , \tag{9b}$$

with A adjusted to remove the overlap with the on-site Coulomb interaction U; the p-wave-like function

$$g_x = \sin p_x \tag{10}$$

along with g_y and g_z; the E_g d-wave-like functions

$$g_{x^2-y^2} = \cos p_x - \cos p_y , \tag{11a}$$

$$g_{3z^2-r^2} = 2 \cos p_z - \cos p_x - \cos p_y , \tag{11b}$$

and the T_{2g} d-wave function

$$g_{xy} = \sin p_x \sin p_y , \tag{12}$$

and its partners g_{xz} and g_{yz}. Naturally, the basis functions can be extended, but for our purposes these will be sufficient. Using these functions to weight the averages in Eq. (3), coupling constants for the various channels are defined by[16]

$$\bar{\lambda}_\alpha = -\frac{\int \frac{d^2p}{|v_p|} \int \frac{d^2p'}{(2\pi)^3 |v_{p'}|} g_\alpha(p') V(p', p) g_\alpha(p)}{\int \frac{d^2p}{|v_p|} g_\alpha^2(p)} . \tag{13}$$

Here, $V = V_3$ for the even-parity channels and $V = V_t$ for the odd-parity channels. It is also useful to introduce a coupling constant λ_z which gives a measure of the wave function and effective-mass renormalization arising from the frequency dependence of the self-energy:

$$\lambda_z = \int \frac{d^2p}{|v_p|} \int \frac{d^2p'}{(2\pi)^3 |v_{p'}|} \left[\frac{U^3 X_0^2(p'-p)}{1 - U X_0(p'-p)} + \frac{U^2 X_0(p'-p)}{1 - U^2 X_0^2(p'-p)} \right] \Bigg/ \int \frac{d^2p}{|v_p|} . \tag{14}$$

Using λ_z, an effective coupling constant for α-wave pairing is defined by

$$\lambda_\alpha = \frac{\bar{\lambda}_\alpha}{1 + \lambda_z} . \tag{15}$$

A rough estimate for T_c^α is given by the BCS expression

$T_c^\alpha = \omega_c \exp(-1/\lambda_\alpha)$ with ω_c a cutoff frequency set by the spectral weight $F(\omega)$.

In the next section we calculate λ_α as a function of μ and U for the SDW effective pairing interactions, Eqs. (7) and (8). We also calculate the spatial Fourier transform of the interaction. This Fourier transform clearly shows

the oscillatory structure[17] of the real-space pairing potential which arises from $V(p',p)$. Section III contains an analysis of the CDW and Peierls interactions, and Sec. IV, the conclusion.

II. THE SDW PAIRING INTERACTION

In order to gain insight into the nature of the SDW-mediated pairing interaction, we have Fourier-transformed the even-parity interaction,

$$V_s(l) = \sum_q e^{i\mathbf{q}\cdot l} V_s(\mathbf{q}) \ . \tag{16}$$

Results for $U = 4$ and $\mu = -1$ and -2.5 are shown in Figs. 2(a) and 2(b), respectively. Here we have arbitrarily normalized the strength of the on-site interaction to unit magnitude. For $U = 4$, $\mu_c = -0.71$, so that Fig. 2(a) corresponds to a band filling which is close to the SDW instability. In this case, the pairing interaction is repulsive on site, as one would expect, but attractive for pairs placed on near-neighbor sites. It is repulsive for next-nearest-neighbor sites, etc. As μ approaches μ_c, this sign pattern persists, and the range of the interaction increases like $[1 - U\chi_0(q^*,\mu)]^{-1/2}$, while its strength goes as $[1 - U\chi_0(q^*,\mu)]^{-1}$. As μ decreases, both the strength and range decrease. In addition, as the wave vectors spanning the Fermi surface decrease, the scale for oscilla-

tions increase, leading at $\mu = -2.5$ to the $V_s(l)$ structure shown in Fig. 2(b). Here the near-neighbor pairing potential is repulsive, while for the next-nearest-neighbor pairing potential it is attractive. From Figs. 2(a) and 2(b) it would appear that when $U = 4$, the $(d_{x^2-y^2}, d_{3z^2-r^2})$-like states are favored for $\mu = -1$, while the (d_{xy}, d_{yz}, d_{xz})-like states are favored for $\mu = -2.5$.

Figures 3(a) and 3(b) show the effective coupling constants λ_α, Eq. (15), versus μ for $U = 4$ and 10. These results were obtained from a numerical evaluation of Eqs. (13) and (14). As U increases, the SDW instability occurs at more negative values of μ. The results for $U = 4$ show that, as μ approaches the SDW instability, $\lambda_{x^2-y^2}$ dominates. The extended s-wave coupling λ_{s^*} also becomes attractive in this region. As μ decreases, the strength of these couplings decreases and at $\mu = -2.2$ the λ_{xy} coupling becomes the most attractive channel. Finally, for $\mu < -3.5$, the triplet p-wave channel becomes the most attractive, although λ_x is very small in magnitude.

When U is increased, the critical value μ_c becomes more negative, and the volume of the Fermi sea decreases. For $U = 6$ and 8, the qualitative behavior of the couplings
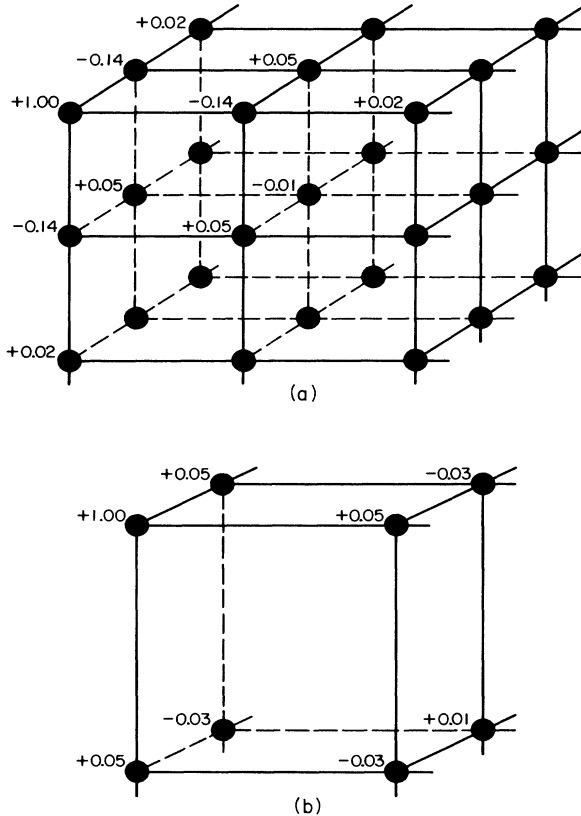
FIG. 2. Even-parity interaction V_s in real space for $U = 4$ and (a) $\mu = -1$ and (b) $\mu = -2.5$. These results have been normalized so that the on-site interaction has unit magnitude.
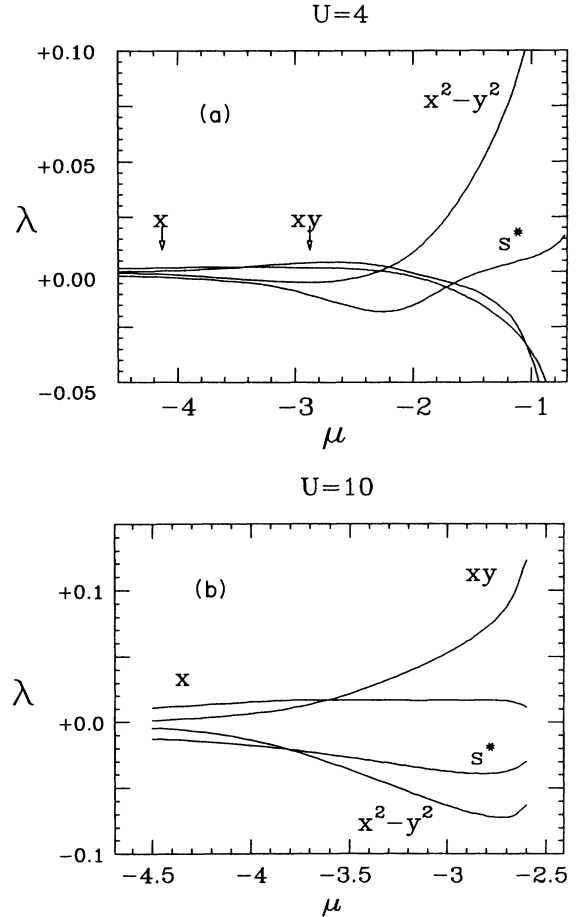
FIG. 3. The effective couplings λ_s, λ_{xy}, $\lambda_{x^2-y^2}$, and λ_x vs μ for (a) $U = 4$ and (b) $U = 10$. Panel (a) was previously shown in Ref. 8 and is reproduced here so that the results for $U = 10$ can be compared to $U = 4$.

is similar to $U=4$, although $\lambda_{x^2-y^2}$ becomes smaller, and λ_{xy} increases relative to the $U=4$ case. When U exceeds 8, a change in behavior occurs and, as shown in Fig. 3(b), for $U=10$, λ_{xy} is dominant near the instability. In this case, $\mu=-2.55$ and the characteristic wave vector spanning the Fermi surface is small enough that the attractive oscillations of the potential near the instability give rise to a potential with the structure shown in Fig. 2(b).

III. CDW AND PEIERLS PAIRING INTERACTIONS

Next, we consider the effect of a near-neighbor Coulomb repulsion

$$\sum_{\langle ij \rangle} V_0 n_i n_j \; . \tag{17}$$

Fourier-transforming this and screening it within the RPA, we have, for the effective interaction,

$$V(q) = \frac{V_0(q)}{1+2\Pi_0(q)V_0(q)} \; . \tag{18}$$

Here,

$$V_0(q) = 2V_0(\cos q_x + \cos q_y + \cos q_z) \; , \tag{19}$$

and $\Pi_0(q)$ is the single-spin RPA polarization. We have chosen a sign convention such that $\Pi_0(q) = \chi_0(q)$, Eq. (5). As discussed, when μ is near 0, $\Pi_0(q)$ peaks for $\mathbf{q}^*$ near (π,π,π). In this regime $V_0(q)$ is negative, and the RPA screened interaction, Eq. (18), exhibits a CDW instability when

$$1+2\Pi_0(q^*)V_0(q^*) = 0 \; . \tag{20}$$

As in the SDW case, we are interested in values of μ less than the critical μ_c at which Eq. (20) is satisfied for $T=0$. This corresponds to a region with strong CDW fluctuations. The CDW mechanism is related to the original work of Kohn and Luttinger,[16,6] using the near nesting of the Fermi surface to enhance the strength of the coupling.

Since $V_0(q^*)$ is negative near the instability, the spatial Fourier transform of the effective interaction, Eq. (18), will have the opposite sign from the SDW case, except for on-site pairing, where it remains repulsive due to the on-site Coulomb interaction U. Note that, here we are interested in the case where the system is near a CDW instability, and we can neglect the paramagnon contribution, retaining only the on-site repulsive Coulomb part. Figure 4 shows the behavior of the effective coupling constants λ_α vs μ for $V_0 = \frac{1}{3}$. Note that as the CDW instability is approached, λ_{xy} dominates, leading to pairing in the $T_{2g}(d_{xy}, d_{yz}, d_{xz})$-like manifold. The E_g coupling constants $\lambda_{x^2-y^2} = \lambda_{3z^2-r^2}$ are negative, corresponding to the near-neighbor repulsion. This change in behavior from the SDW-mediated interaction arises from the fact that $V_0(q^*)$ is negative as discussed above.

We have modeled an electron-phonon interaction at zero frequency by

$$V(q) = \frac{2|g_q|^2\omega_q}{-\omega_q^2 + 2\omega_q|g_q|^2\Pi_0(q)} \; . \tag{21}$$
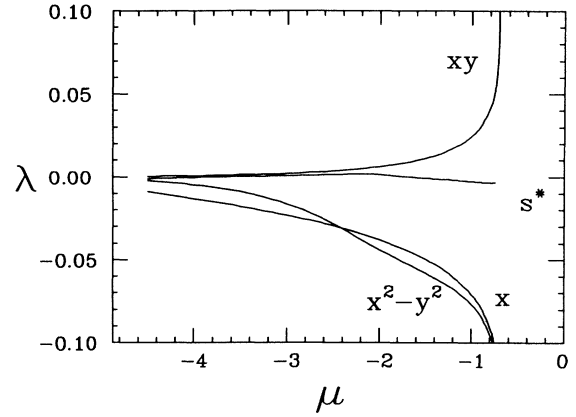
FIG. 4. Effective couplings vs μ for a system with a CDW instability.

Setting $g = 2|g_q|^2/\omega_q$, this becomes

$$V(q) = -\frac{g}{1-g\Pi_0(q)} \; , \tag{22}$$

which exhibits a Peierls instability when the denominator vanishes. Once again we select $\mu < \mu_c$ so that the system is stable but has a low-lying phonon mode for q^* near (π,π,π). The coupling constants λ_α for $g=4$ are shown versus μ in Fig. 5. We continue to assume that there is an on-site Coulomb interaction which suppresses the usual s-wave pairing. In practice, dynamic screening gives a reduced on-site Coulomb pseudopotential which may be such that the s-wave pairing associated with $g_0(p)=1$ becomes important.

IV. CONCLUSIONS

Systems near Fermi-surface instabilities have low-lying boson excitations characterized by wave vectors which connect the nearly nested regions of the Fermi surface. The exchange of these excitations can lead to pairing potentials which are attractive in the even-parity channel.
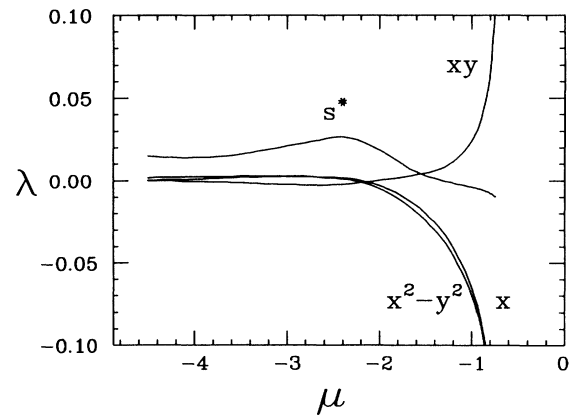
FIG. 5. Effective couplings vs μ for a system with a Peierls instability.

In particular, if on-site pairing is unfavorable due to Coulomb repulsion, d-wave and extended s-wave pairing may occur. Within a RPA approximation of the effective interaction, we have evaluated the effective coupling constant for SDW, CDW, and Peierls interactions. This has been done for both the low-angular-momentum singlet and triplet channels. We find that near half-filling for a SDW, the $E_g(d_{x^2-y^2}, d_{3z^2-x^2-y^2})$ manifold is favored, while for CDW and Peierls interactions the $T_{2g}(d_{xy}, d_{yz}, d_{xz})$ manifold is favored. However, even with the enhancement associated with a nearly nested Fermi surface the effective coupling is relatively weak. In addition, as we have noted, the RPA approximation overestimates it near μ_c, where fluctuations associated with the instability will act to reduce it. Thus, just as for ^{3}He, the RPA paramagnon approximation provides a model which exhibits the phenomena, but further work will be needed to obtain reliable estimates of T_c.

Naturally, a key question is to what extent can the type of weak-coupling RPA approach presented here be applied to real materials? Is the pairing interaction sufficiently strong or does the pairing in the heavy-fermion superconductors and Bechgaard salts arise from a strong-coupling limit in which U is large compared to the bandwidth? In this case, for a non-half-filled band the charge degrees of freedom are coupled through the spin fluctuations and again one finds anisotropic pairing.[7] Clearly, we need more detailed calculations for both the weak-coupling and strong-coupling limits. Our goals in this paper were (1) to generalize the weak-coupling RPA approach for the SDW-mediated interaction[8] to treat CDW- and Peierls-mediated interactions in the presence of a repulsive on-site U interaction, and (2) to clarify the physical origin of the attractive d-wave interaction which these lead to near a Fermi-surface instability.

*Present address: Los Alamos National Laboratory, P.O. Box 1663, Los Alamos, NM 97545.

[1]L. P. Gorkov and O. N. Dorokhov, J. Low Temp. Phys. **22**, 1 (1976); Zh. Eksp. Teor. Fiz. **65**, 1658 (1973) [Sov. Phys.—JETP **38**, 830 (1974)].

[2]G. Bilbro and W. L. McMillan, Phys. Rev. B **14**, 1887 (1976).

[3]C. Z. Balseiro and L. M. Falicov, Phys. Rev. B **20**, 4457 (1979).

[4]G. Aeppli, A. Goldman, G. Shirane, E. Bucher and M.-Ch. Lux-Steiner, Phys. Rev. Lett. **58**, 808 (1987); A. P. Ramirez, B. Batlogg, E. Bucher, and A. S. Cooper, Phys. Rev. Lett. **57**, 1072 (1986).

[5]D. Jerome, J. Phys. (Paris) Colloq. **44**, C3-755 (1983).

[6]V. J. Emery, J. Phys. (Paris) Colloq. **44**, C3-977 (1983); Synth. Met. **13**, 21 (1986).

[7]J. E. Hirsch, Phys. Rev. Lett. **54**, 1317 (1985).

[8]D. J. Scalapino, E. Loh, Jr., and J. E. Hirsch, Phys. Rev. B **34**, 8190 (1986).

[9]K. Miyake, S. Schmitt-Rink, and C. M. Varma, Phys. Rev. B **34**, 6554 (1986).

[10]M. T. Béal-Monod, C. Bourbonnais, and V. J. Emery, Phys. Rev. B **34**, 7716 (1986).

[11]The variation of the p-wave coupling with band filling in the paramagnon model was discussed by D. J. Scalapino, Condensed Matter Physics, The Theodore D. Holstein Symposium, 1986 (Springer-Verlag, Berlin, 1986).

[12]A. Auerbach and K. Levin, Phys. Rev. Lett. **57**, 877 (1986).

[13]M. Lavagna, A. J. Millis, and P. A. Lee, Phys. Rev. Lett. **58**, 266 (1987).

[14]G. M. Eliashberg, JETP Lett. **11**, 696 (1960).

[15]D. J. Scalapino, in Superconductivity, edited by R. D. Parks (Dekker, New York, 1968), Chap. 7.

[16]The $(2\pi)^{-3}$ factor was inadvertently left out in the expression for λ in Ref. 8. However, it was correctly included in the numerical results reported there.

[17]W. Kohn and J. M. Luttinger, Phys. Rev. Lett. **15**, 524 (1965).